TESTS OF THE STANDARD MODEL AT LEP

Chris Hawkes
CERN, European Organisation for Particle Physics,
1211 Geneva 23, Switzerland

ABSTRACT

Measurements made by the four LEP experiments of electroweak parameters and the strong coupling constant are presented. These are used in an overall Standard Model fit and a constraint on the mass of the top quark is derived.

1. Precision Measurements of Electroweak Parameters

During 1989, 1990 and 1991 the four main experiments at the LEP e^+e^- collider (ALEPH, DELPHI, L3 and OPAL) have recorded data representing a total of approximately 1.8×10^6 multihadronic decays of the Z^0. These data have been used to measure many parameters of the electroweak sector of the Standard Model. The results presented in this review are preliminary and give the status of the analyses at the time of the 1992 SLAC Summer Institute.

1.1 LEP Beam Energy Calibration

A precise calibration of the LEP beam energy is vital for the measurement of the mass, M_Z, and width, Γ_Z, of the Z^0. During 1991 this was done, for the first time at LEP, by the method of resonant spin depolarisation [1].

When a beam circulates freely in a storage ring it tends to become transversely polarised due to synchrotron radiation. Such transverse polarisation has been measured during single-beam operation at LEP several times at the level of 5-16%. This can be exploited to calibrate the beam energy by using an oscillating magnetic field to induce a resonant depolarisation. The frequency of the magnetic field is scanned and depolarisation occurs when it matches the spin precession frequency of the circulating electrons.

The beam energy, E_B is given by:

$$E_B = \frac{m_e c^2}{a_e} \nu_s$$

where m_e is the electron mass, c is the speed of light, a_e is the precisely measured gyromagnetic anomaly of the electron and ν_s is the number of spin precessions made by the electrons during each revolution of the LEP ring. The resonant frequency of the magnetic field measures the non-integer part of ν_s.

This has been used to determine the centre-of-mass energy, $\sqrt{s}$, to a precision of ± 1 MeV at the time of measurement. So far this calibration has been made only under special conditions during periods of machine development. Larger uncertainties arise in the derivation of $\sqrt{s}$ during LEP fills used for physics, due to instabilities.

Tidal variations caused by the moon and the sun lead to distortions of the earth's crust resulting in minor variations of the dimensions of the LEP ring. This results in a scatter in the results for $\sqrt{s}$ deduced from four separate polarisation runs. In principle this effect can be corrected for when it has been better understood. For the moment it leads to a systematic uncertainty of ± 3.7 MeV in $\sqrt{s}$.

Measurements of magnets under laboratory conditions and in the LEP tunnel have shown that, due to their method of construction, the magnetic field, and hence the beam energy, depends on the temperature. The variation of temperature during LEP operation leads to a ± 3 MeV uncertainty on $\sqrt{s}$.

Direct measurements of the flux in the LEP magnets are made at regular intervals. These show an additional drift with time which cannot be accounted for by other effects and contributes ± 2 MeV to the error on $\sqrt{s}$.

It has recently been discovered that $\sqrt{s}$ at the L3 and OPAL interaction points is about 15 MeV higher than that at ALEPH and DELPHI. This is due to a longitudinal misalignment of the RF cavities which are positioned on each side of L3 and OPAL. After correction, there remains a ± 1 MeV uncertainty in $\sqrt{s}$ due to this.

Combining these and some smaller effects leads to an expected systematic error of ± 7 MeV on M_Z from the 1991 LEP data [2].

This 1991 M_Z measurement was not available at the time of the conference and so the published value [3] based on 1990 LEP data has been used in this review: $M_Z^{1990} = 91.175 \pm 0.021$ GeV.

1.2 Z^0 Line Shapes

The cross sections, as a function of $\sqrt{s}$ around M_Z, have been measured for $e^+e^- \to$ hadrons, e^+e^-, $\mu^+\mu^-$, $\tau^+\tau^-$ [4]. The cross sections are given by:

$$\sigma = \frac{N - N_B}{\epsilon \int \mathcal{L}\, dt}$$

where N is the number of events selected, N_B is the number of background events, ϵ is the efficiency and $\int \mathcal{L}\, dt$ is the integrated luminosity, measured by counting low angle Bhabha scattering events. These measurements benefit from the small statistical errors resulting from the large LEP data samples, but require correspondingly small systematic errors. The background component is typically $O(0.1\%)$ for hadrons, e^+e^- and $\mu^+\mu^-$ and $O(1\%)$ for $\tau^+\tau^-$. The uncertainty from the luminosity is less than 1%, with a component of 0.3% from theory.

1.3 Forward-Backward Charge Asymmetries

The forward-backward charge asymmetry, A_{FB}, has been measured as a function of $\sqrt{s}$ for $e^+e^- \to e^+e^-, \mu^+\mu^-, \tau^+\tau^-$ [4]. This is defined by:

$$A_{FB} = \frac{N_F - N_B}{N_F + N_B}$$

where N_F is the number of forward events ($0° < \theta < 90°$) and N_B is the number of backward events ($90° < \theta < 180°$). The polar angle, θ, is between the μ^+ and e^+ directions. In practice, A_{FB} is usually derived from a fit to the differential cross section, $d\sigma/d\cos\theta$.

At present, the systematic errors, from charge and angle measurement, are much smaller than the statistical errors ($O(1\%)$ for each channel for each experiment).

1.4 Fitting the Data

Within the Standard Model, the differential cross section for $e^+e^- \to l^+l^-$ can be written as the Improved Born Approximation (IBA) [5]:

$$\frac{2s}{\pi\alpha^2} \cdot \frac{d\sigma}{d\cos\theta}(e^+e^- \to l^+l^-) =$$

$$\left(\frac{1}{1-\Delta\alpha}\right)^2 (1+\cos^2\theta)$$

$$+4\mathrm{Re}\left\{\frac{2}{1-\Delta\alpha}\chi(s)\left[\hat{g}_v^e \hat{g}_v^l (1+\cos^2\theta) + 2\hat{g}_a^e \hat{g}_a^l \cos\theta\right]\right\}$$

$$+16|\chi(s)|^2\left[(\hat{g}_a^{e\,2} + \hat{g}_v^{e\,2})(\hat{g}_a^{l\,2} + \hat{g}_v^{l\,2})(1+\cos^2\theta) + 8\hat{g}_a^e \hat{g}_v^e \hat{g}_a^l \hat{g}_v^l \cos\theta\right]$$

where

$$\chi(s) = \frac{G_F M_Z^2}{8\pi\alpha\sqrt{2}} \cdot \frac{s}{s - M_Z^2 + is\Gamma_Z/M_Z}$$

G_F is the Fermi coupling constant, α is the fine structure constant and $\Delta\alpha$ is the QED vacuum polarisation correction.

In the IBA the effects of higher order corrections are largely absorbed into the definitions of $\hat{g}_a^l$ and $\hat{g}_v^l$, the effective axial and vector couplings at the $Z^0 l^+ l^-$ vertex. These are functions of α, G_F, M_Z and also, due to vacuum polarisation and vertex corrections, of the top quark mass, m_t, and the Higgs mass, M_H. With these definitions the simple "Born level" dependence of the total cross section, σ_{TOT}, and A_{FB} on the couplings is recovered.

The three lines of the IBA as written above correspond to a γ-exchange term, which is small for $\sqrt{s}$ near to M_Z; a Z^0-γ interference term and a Z^0 exchange term. The interference term has a symmetric component, proportional to $1 + \cos^2\theta$, which gives a small contribution to σ_{TOT} away from the Z^0 peak, and an antisymmetric component, proportional to $\cos\theta$, which controls the $\sqrt{s}$ dependence of A_{FB}. The Z^0 exchange term has a symmetric component, which leads to the Z^0 line shape, and an antisymmetric component, which gives the forward-backward asymmetry on the Z^0 peak.

At $\sqrt{s} = M_Z$, the total cross section:

$$\sigma_{TOT} \propto (\hat{g}_a^{e\,2} + \hat{g}_v^{e\,2})(\hat{g}_a^{l\,2} + \hat{g}_v^{l\,2}) \propto \Gamma_{ee}\Gamma_{l^+l^-}$$

where Γ_{ee} and $\Gamma_{l^+l^-}$ are the partial decay widths of the Z^0 to e^+e^- and l^+l^- respectively, and the forward-backward asymmetry:

$$A_{FB}(\sqrt{s} = M_Z) \propto \frac{\hat{g}_a^e \hat{g}_v^e \hat{g}_a^l \hat{g}_v^l}{(\hat{g}_a^{e\,2} + \hat{g}_v^{e\,2})(\hat{g}_a^{l\,2} + \hat{g}_v^{l\,2})} \quad .$$

These depend on both initial and final state couplings.

There are additional corrections to the IBA. Photonic corrections, due to initial and final state radiation, have a large effect, but are well understood. QCD corrections, due to the emission of gluons from quarks in the final state, lead to a correction of $O(1 + \alpha_S/\pi)$ to the ratio, R_Z, of hadronic to leptonic cross sections. For $e^+e^- \to e^+e^-$ there are t-channel contributions producing a peak in the forward direction. There are also higher order corrections from vacuum polarisation, vertex correction and box diagrams. These are largely absorbed into the definitions of the effective couplings but they do lead to the sensitivity of the measurements to "virtual physics" effects, such as m_t and M_H.

All of these contributions are included in the Standard Model fitting programs used by the LEP collaborations to fit their line shape and forward-backward asymmetry data [6]. An example is presented in Figs. 1-2 from the L3 Collaboration.

Figure 1 shows the lepton pair cross sections and Fig. 2 the forward-backward asymmetries, for 1990 and 1991 data. The curves are the result of a single Standard Model fit to all of these data with five free parameters: M_Z, Γ_Z, Γ_{had}, $\hat{g}_a^l$ and $\hat{g}_v^l$.

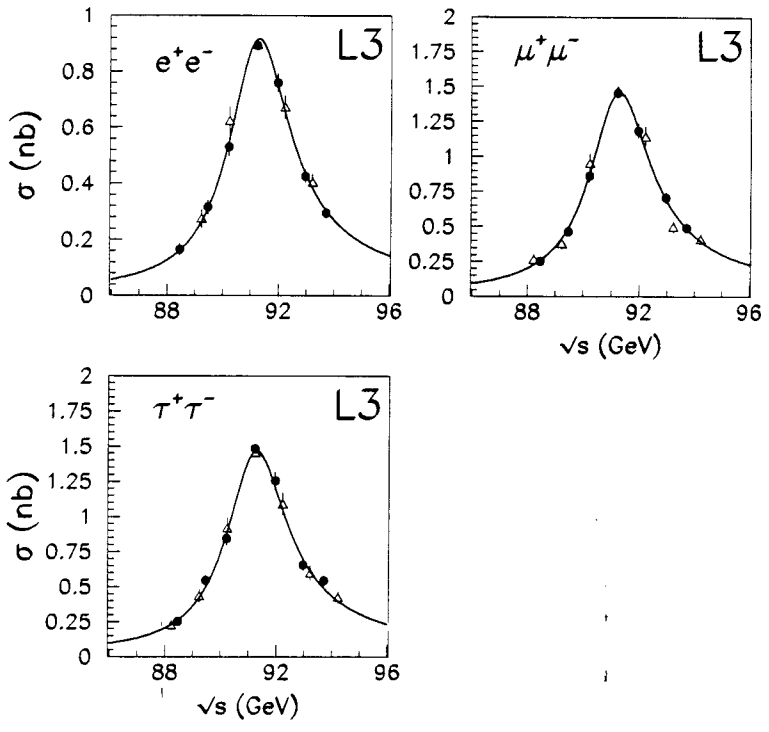

Figure 1: Lepton pair cross sections measured by the L3 Collaboration from 1990 (triangles) and 1991 (circles) data. The t-channel contribution has been subtracted from the $e^+e^- \to e^+e^-$ data. The curve is the result of a five parameter Standard Model fit to these and the lepton pair forward-backward asymmetry data.

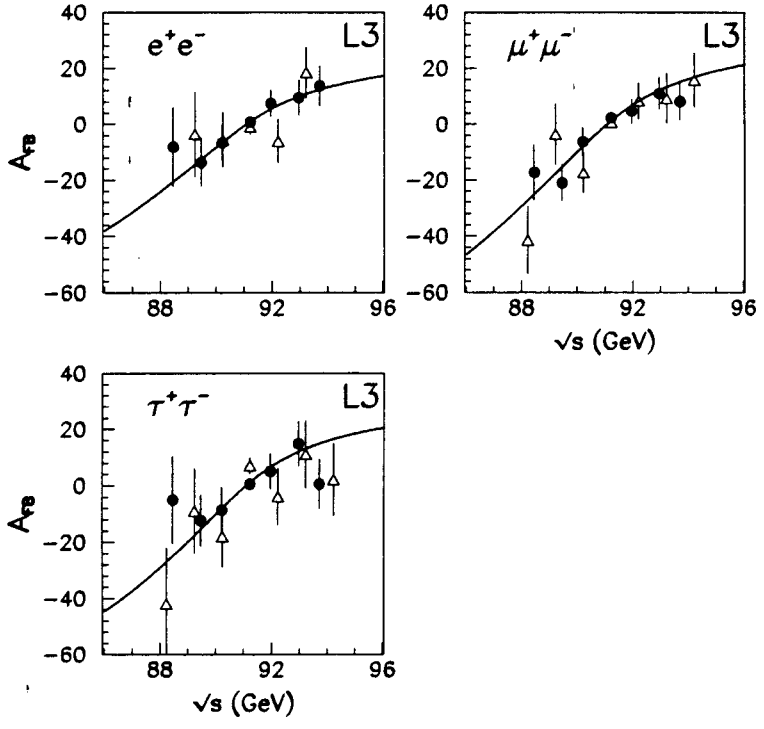

Figure 2: Lepton pair forward-backward charge asymmetries measured by the L3 Collaboration from 1990 (triangles) and 1991 (circles) data. The t-channel contribution has been subtracted from the $e^+e^- \to e^+e^-$ data. The curve is the result of a five parameter Standard Model fit to these and the lepton pair cross section data.

1.5 Combining LEP Data

The four LEP collaborations have used technically different fitting procedures and extracted different sets of electroweak parameters from their data. In reference [3] the effects of these differences on results from combined LEP data were studied. It was concluded that, at the present level of precision, these differences are unimportant and a simple averaging procedure is adequate, provided correlations are taken into account.

The LEP measurements and a combined LEP average result are shown in Figs. 3-15 for several electroweak parameters. As an illustration, Fig. 3 shows the total width of the Z^0, Γ_Z. First the four individual LEP measurements are given. The errors are those quoted by the collaborations, but with the component which is correlated between the four collaborations subtracted off. For Γ_Z this is estimated to be 5 MeV and comes from the point-to-point LEP beam energy uncertainty. A simple combined LEP average, without the correlated error, is shown below, together with a chi-squared per degree-of-freedom value to indicate the consistency of the input measurements. Below this is the final LEP average result after adding back on the correlated component of the error. At the bottom is shown the Standard Model prediction for Γ_Z. This is not absolute, since it depends on parameters α_S, m_t and M_H. The plot shows the variation with m_t and the shaded bands indicate the variation over the ranges $0.11 \leq \alpha_S \leq 0.13$ and $50 \leq M_H \leq 1000$ GeV. (The combined LEP 95% confidence level lower bound from direct searches for the minimal Standard Model Higgs particle is $M_H > 59$ GeV [7].) These predictions have been calculated using the ZFITTER program [6].

Figure 3 shows that Γ_Z has a substantial m_t dependence. However, it also has a significant α_S and M_H dependence, so that the LEP measurement of Γ_Z is still consistent with quite a wide range of m_t.

The LEP measurements of the charged leptonic partial decay widths of the Z^0 are shown Figs. 4-6. The electronic width has the smallest error since it enters through the initial state in all $e^+e^- \to Z^0 \to f\bar{f}$ events. The correlated component of the systematic error is 0.25% arising partly from the common error on Γ_Z and partly from the theoretical part of the error in the luminosity determination. Since the individual leptonic widths are consistent with one another, lepton universality can be assumed leading to a more precise value for $\Gamma_{l^+l^-}$, as shown in Fig. 7. The m_t dependence of the Standard Model prediction for $\Gamma_{l^+l^-}$ is large, whereas the M_H dependence is quite small and it is independent of α_S. Hence, the LEP measurement of $\Gamma_{l^+l^-}$ places a strong constraint on m_t and is largely responsible for the range of m_t which emerges from the overall Standard Model fit which will be presented in Section 3.

The partial decay width of the Z^0 to multihadronic final states, Γ_{had} (Fig. 8), favours somewhat higher m_t values, but has a large α_S dependence. In a fit in which both m_t and α_S are allowed to vary, lower m_t values can be compensated

by higher α_S values. Hence the cross section data lead to $\alpha_S > 0.12$, the value measured from QCD studies (see Section 2) and used for the Standard Model predictions. This can be seen more clearly in Fig. 9 which shows the effective cross section for $e^+e^- \to$ hadrons at $\sqrt{s} = M_Z$, after unfolding initial-state radiation:

$$\sigma_{had}^{pole} \equiv \frac{12\pi}{M_Z^2} \cdot \frac{\Gamma_{l^+l^-}\Gamma_{had}}{\Gamma_Z^2} \quad .$$

Since $\Gamma_{l^+l^-}$ is independent of α_S, and Γ_{had} and Γ_Z both increase with increasing α_S, σ_{had}^{pole} decreases with increasing α_S. The Standard Model prediction is almost independent of m_t and M_H, so that σ_{had}^{pole} can be interpreted as a direct measurement of α_S. The combined LEP average lies slightly below the prediction, again indicating that the data favour a higher value of α_S. There is a correlated component of the systematic error on σ_{had}^{pole} arising from the theoretical error in the luminosity determination. By taking the ratio $R_Z = \Gamma_{had}/\Gamma_{l^+l^-}$ (Fig. 10) the luminosity measurement cancels out.

The Z^0 partial width to invisible final states, $\Gamma_{inv} = \Gamma_Z - \Gamma_{had} - 3\Gamma_{l^+l^-}$, can also be deduced from the data. It is useful to express this as the ratio:

$$\frac{\Gamma_{inv}}{\Gamma_{l^+l^-}} \equiv \sqrt{\frac{12\pi R_Z}{M_Z^2 \sigma_{had}^{pole}}} - R_Z - 3$$

(Fig. 11) for which many systematics cancel out. Within the Standard Model Γ_{inv} comes only from Z^0 decays to neutrinos, and $\Gamma_{\nu\bar{\nu}}/\Gamma_{l^+l^-} = 1.993 \pm 0.004$, where the error comes from the variation of the top quark mass over the range $90 < m_t < 200$ GeV. Hence, the combined LEP average measurement leads to an effective number of light neutrino species:

$$N_\nu = \frac{\Gamma_{inv}/\Gamma_{l^+l^-}}{\Gamma_{\nu\bar{\nu}}/\Gamma_{l^+l^-}} = 3.04 \pm 0.04 \quad .$$

The data are consistent with the Standard Model with three generations and no additional contributions to the invisible width.

The results can also be expressed in terms of the effective axial and vector couplings. Since $\Gamma_{l^+l^-} \propto \hat{g}_a^{l\,2} + \hat{g}_v^{l\,2}$, and for charged leptons $\hat{g}_v^{l\,2}$ is very small, then $\hat{g}_a^{l\,2}$ is almost completely determined by $\Gamma_{l^+l^-}$ (Fig. 12). Having fixed $\hat{g}_a^{l\,2}$ from the lepton pair cross section measurements, $\hat{g}_v^{l\,2}$ is determined by A_{FB} measured at the Z^0 peak (Fig. 13):

$$A_{FB}^{l\bar{l}}(\sqrt{s} = M_Z) \propto \left(\frac{\hat{g}_a^l \hat{g}_v^l}{\hat{g}_a^{l\,2} + \hat{g}_v^{l\,2}}\right)^2 \approx \left(\frac{\hat{g}_v^l}{\hat{g}_a^l}\right)^2 \quad .$$

This is another important constraint on m_t, since the prediction is independent of α_S.

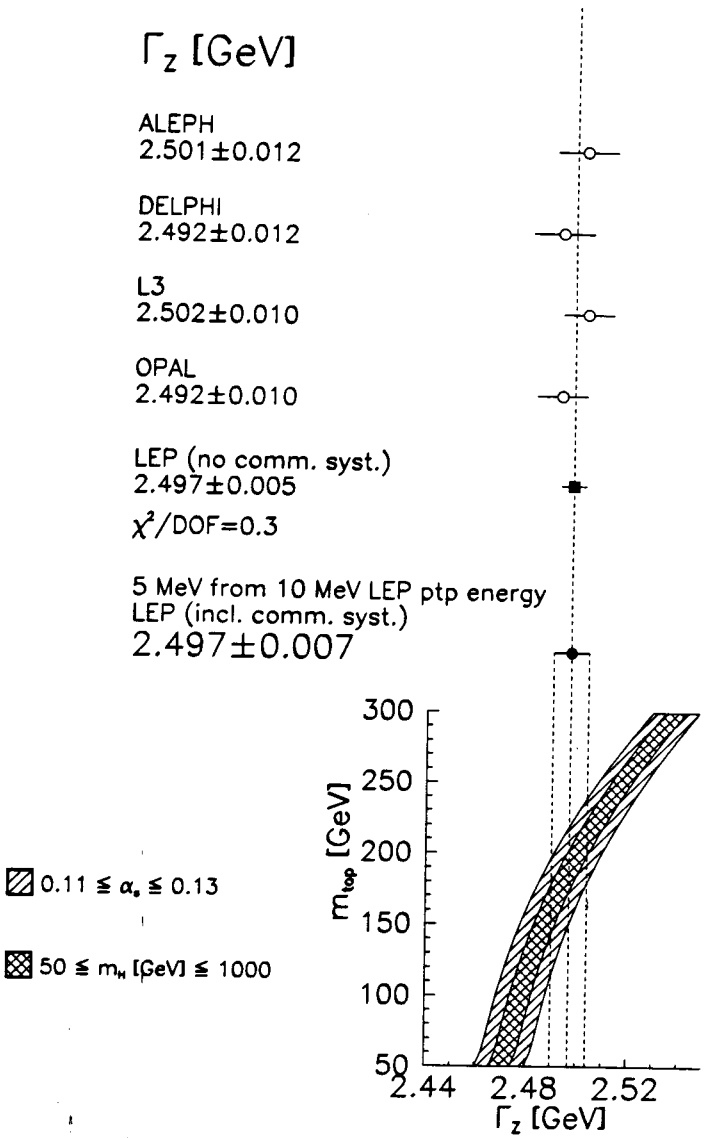

Figure 3: LEP measurements of Γ_Z, the total decay width of the Z^0. See text for details.

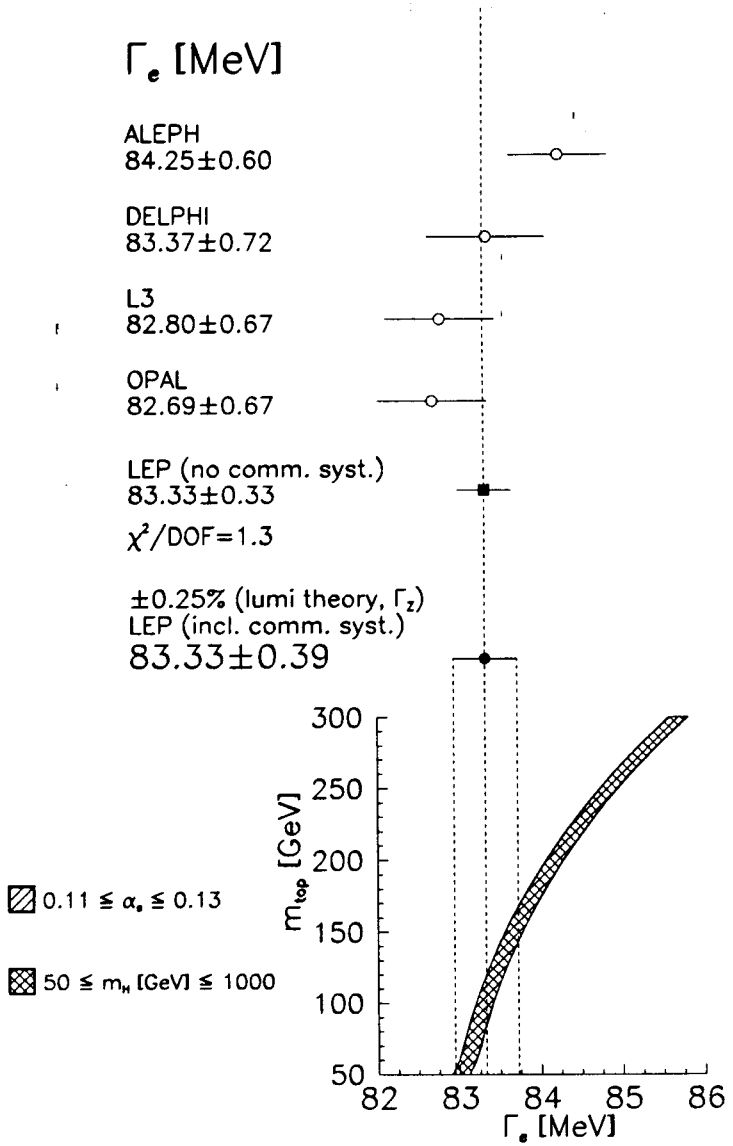

Figure 4: LEP measurements of Γ_{ee}, the partial decay width of the Z^0 to e^+e^-.

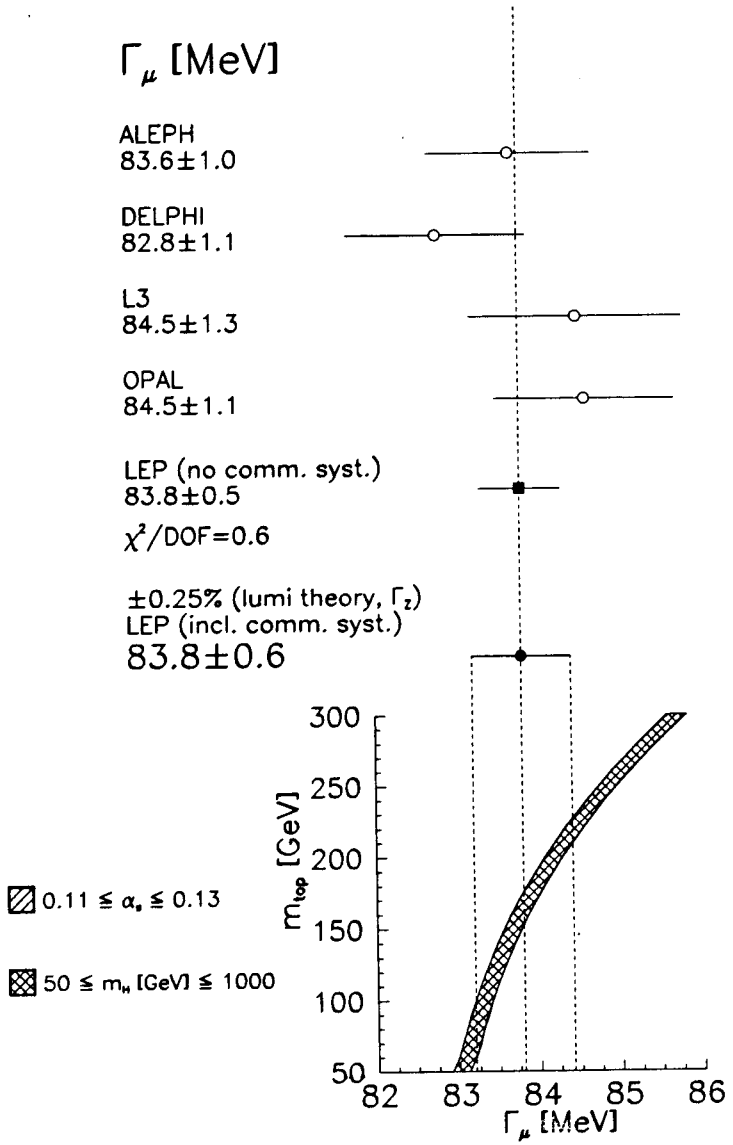

Figure 5: LEP measurements of $\Gamma_{\mu\mu}$, the partial decay width of the Z^0 to $\mu^+\mu^-$.

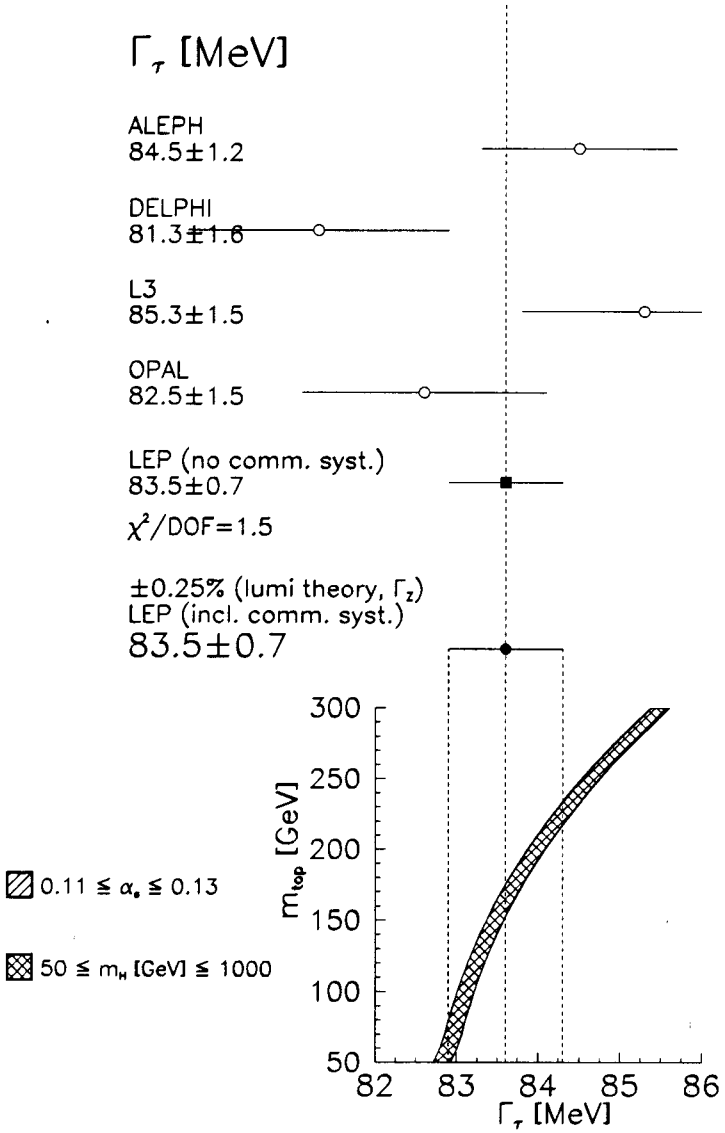

Figure 6: LEP measurements of $\Gamma_{\tau\tau}$, the partial decay width of the Z^0 to $\tau^+\tau^-$.

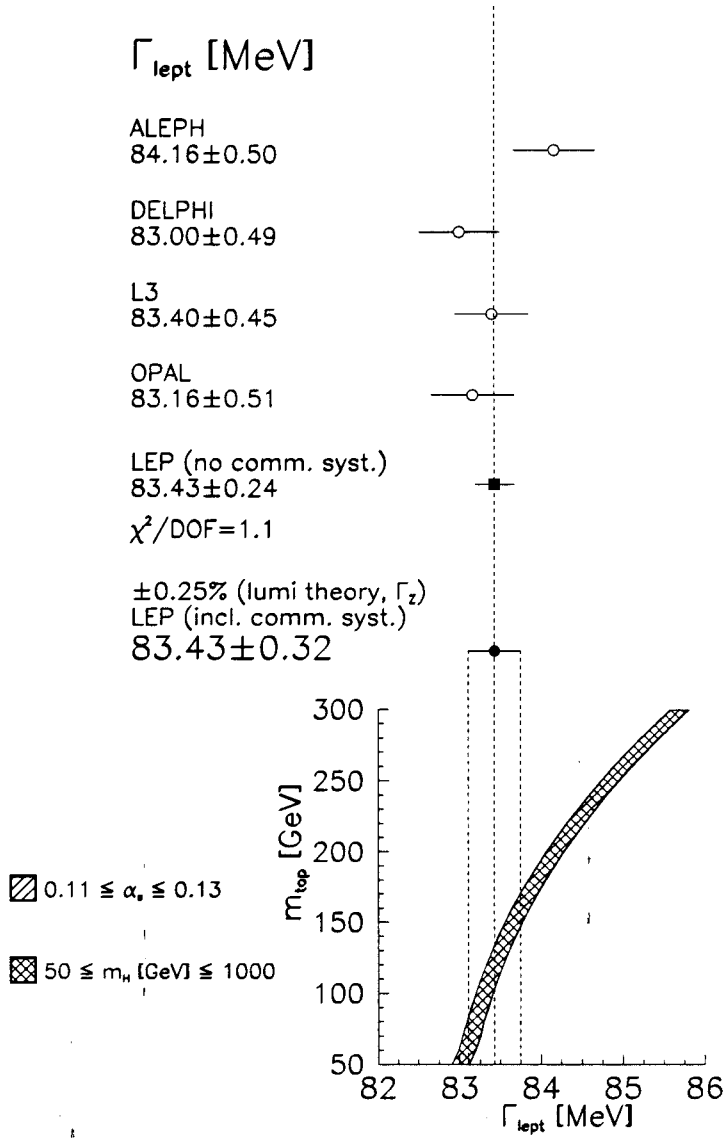

Figure 7: LEP measurements of $\Gamma_{l^+l^-}$, the partial decay width of the Z^0 to l^+l^-, assuming lepton universality.

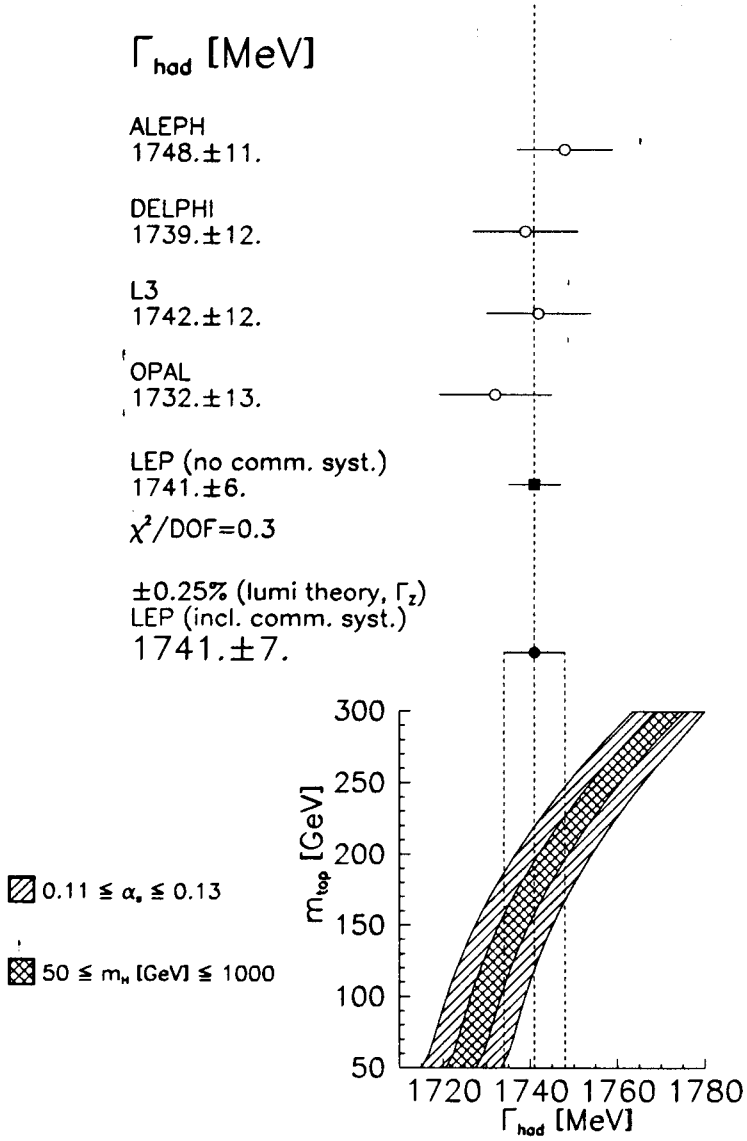

Figure 8: LEP measurements of Γ_{had}, the partial decay width of the Z^0 to multi-hadronic final states.

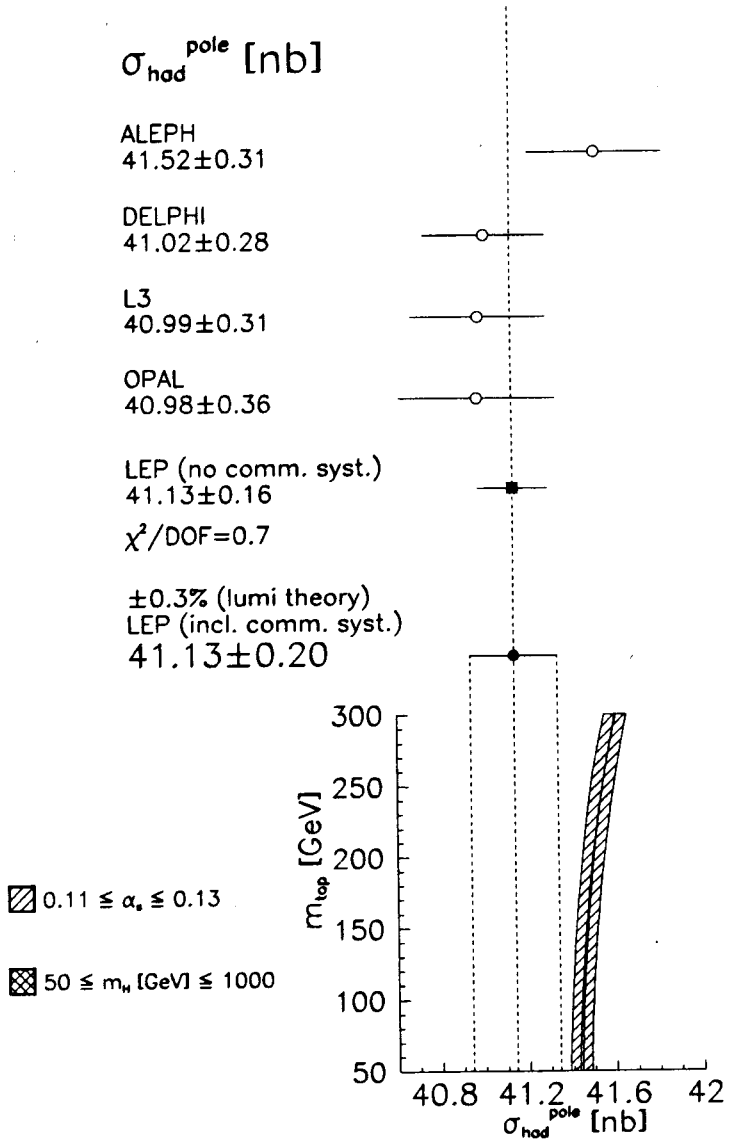

Figure 9: LEP measurements of σ_{had}^{pole}, the peak cross section for $e^+e^- \rightarrow$ hadrons after unfolding initial-state radiation.

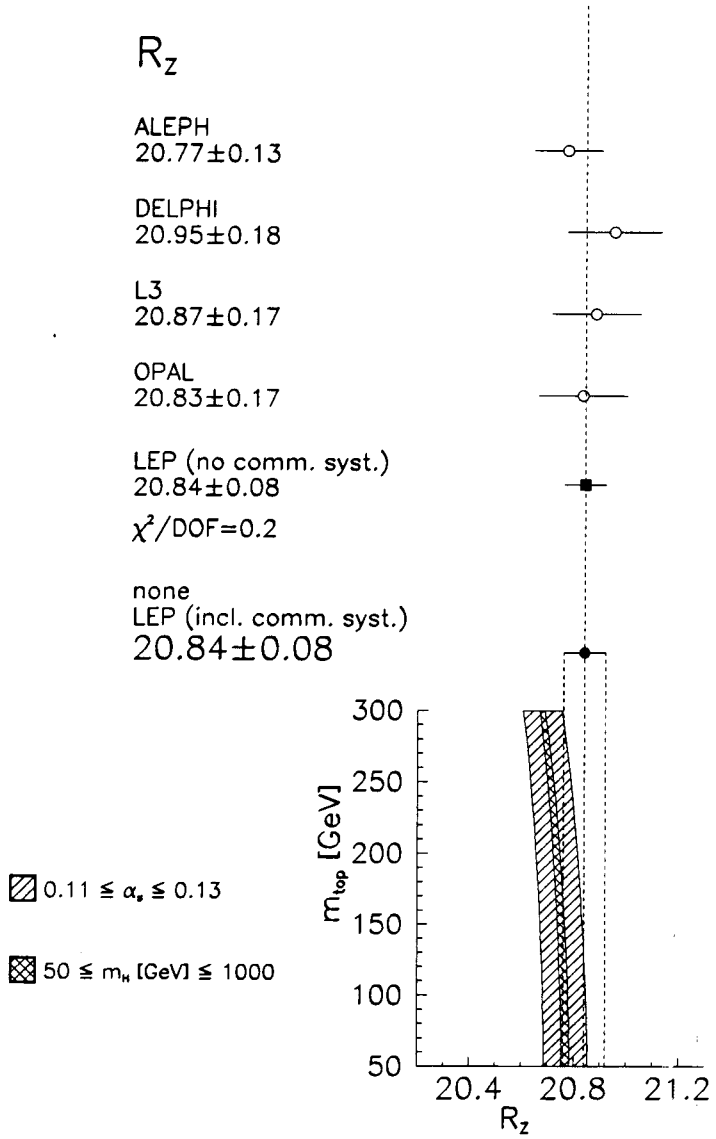

Figure 10: LEP measurements of $R_Z = \Gamma_{had}/\Gamma_{l^+l^-}$.

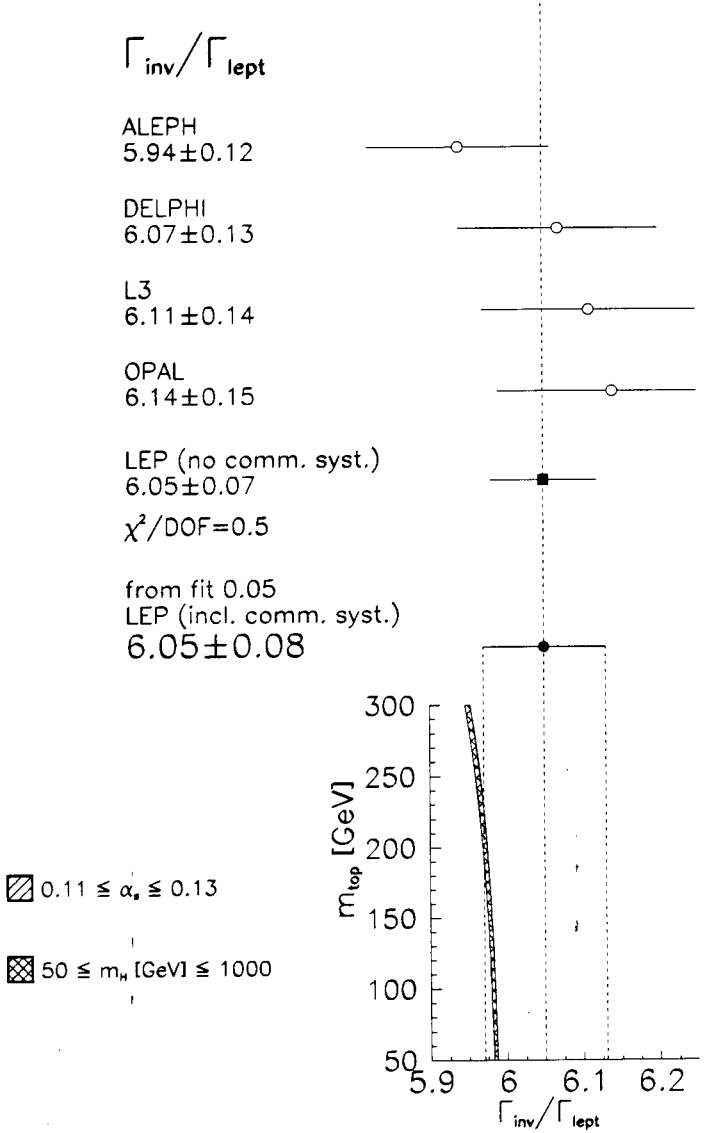

Figure 11: LEP measurements of Γ_{inv}, the partial decay width of the Z^0 to invisible final states.

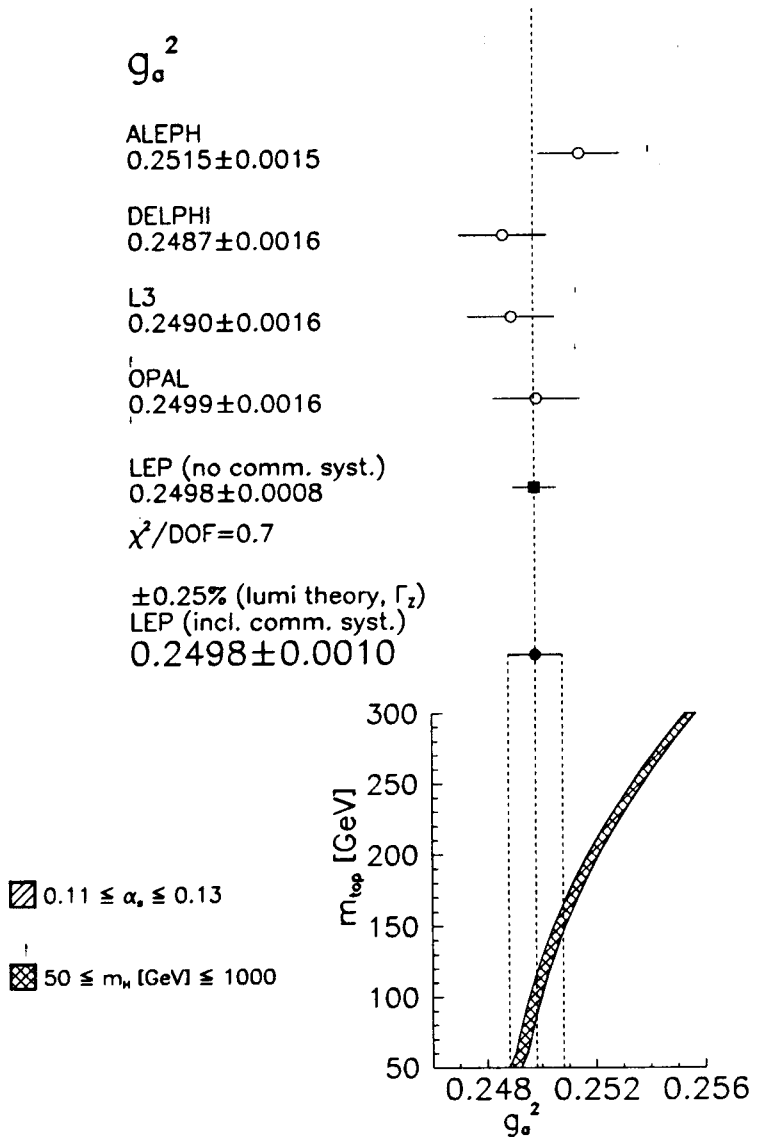

Figure 12: LEP measurements of $\hat{g}_a^{l\,2}$, the square of the effective axial coupling of the Z^0 to l^+l^-.

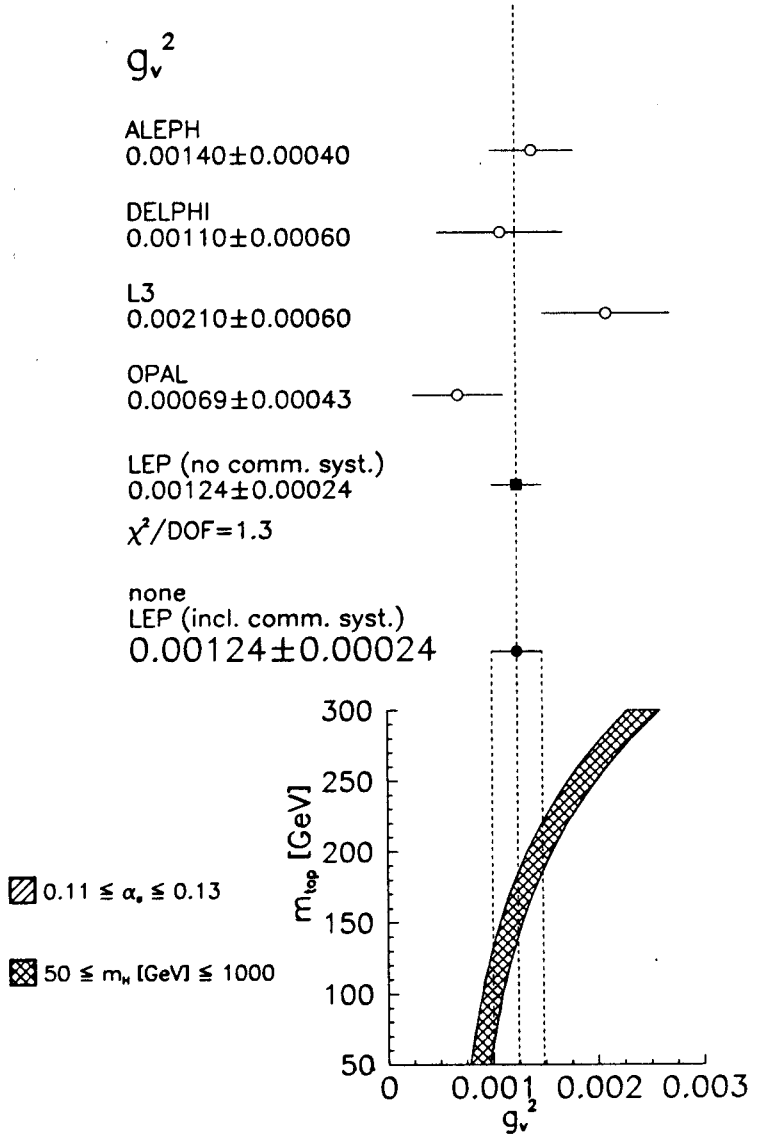

Figure 13: LEP measurements of $\hat{g}_v^{l\,2}$, the square of the effective vector coupling of the Z^0 to l^+l^-.

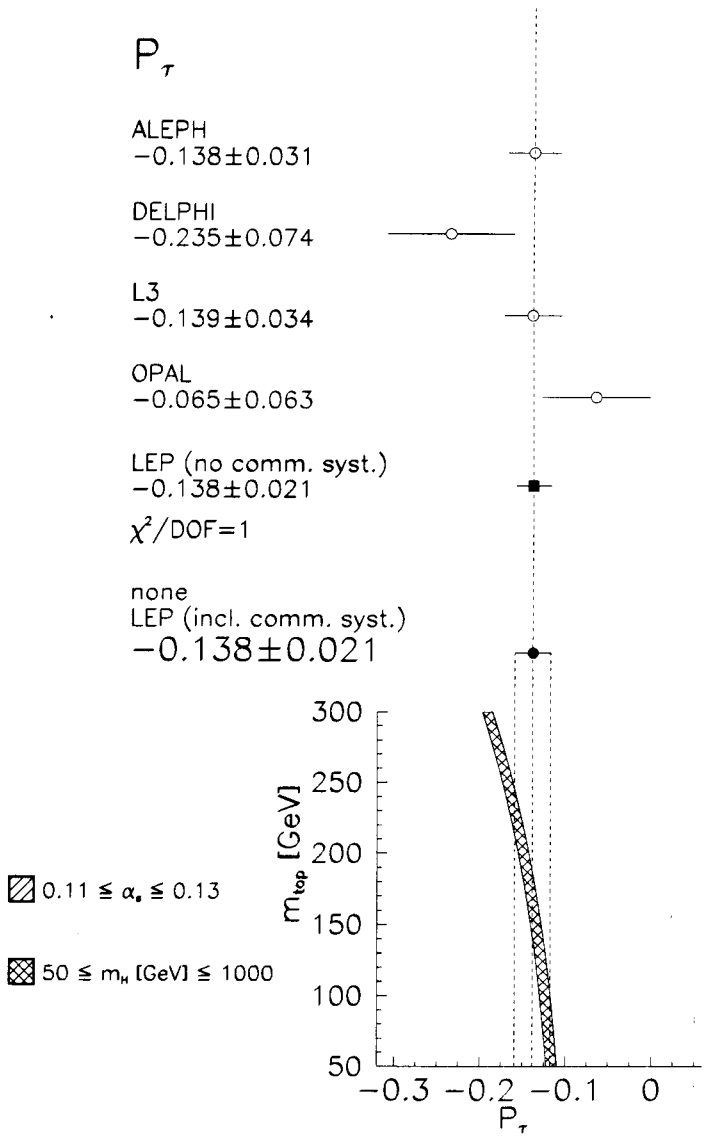

Figure 14: LEP measurements of P_τ, the τ polarisation asymmetry.

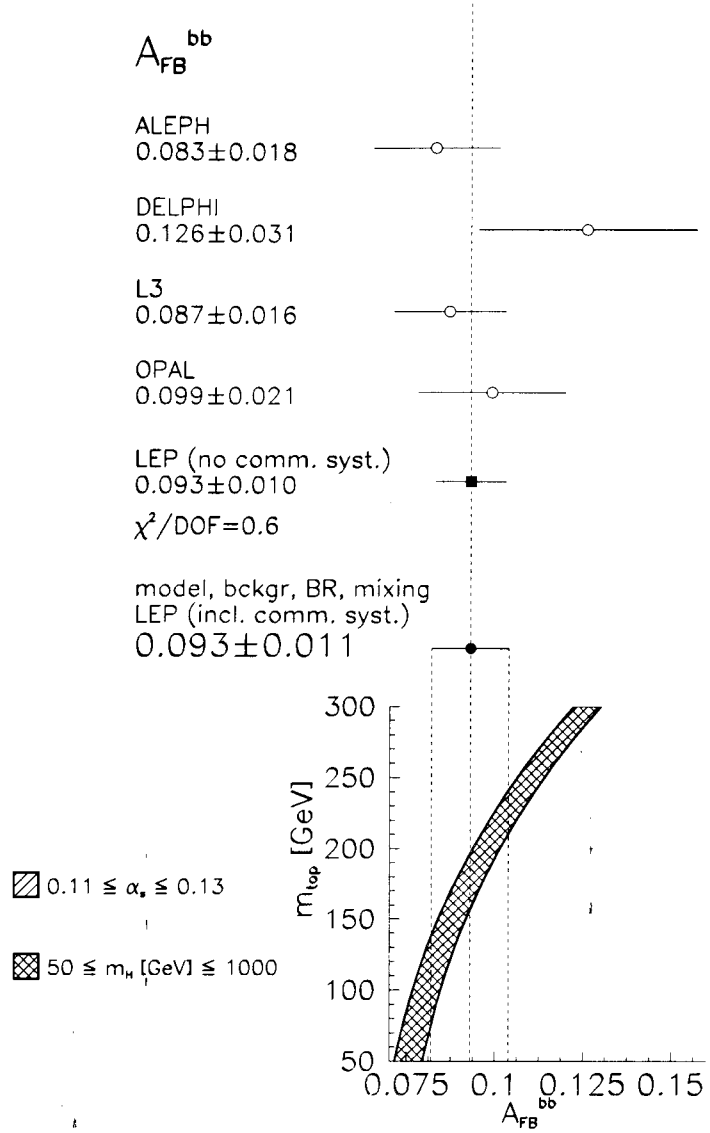

Figure 15: LEP measurements of $A_{FB}^{b\bar{b}}$, the forward-backward charge asymmetry, at $\sqrt{s} = M_Z$, for $e^+e^- \to b\bar{b}$, after correction for $B^0\overline{B}^0$ mixing.

1.6 Tau Polarisation Asymmetry

Due to parity violation in the weak interaction, the tau leptons produced in $e^+e^- \to \tau^+\tau^-$ near $\sqrt{s} = M_Z$ are longitudinally polarised. This can be measured by using the tau decay products as a polarimeter. Tau decays to e, μ, π, K, ρ and a_1 have all been used by the LEP collaborations. For example, in $\tau \to \pi\nu$ decays, the angular distribution of the pions is given by:

$$\frac{1}{N} \cdot \frac{dN}{d\cos\theta} = \frac{1}{2}(1 + P_\tau \cos\theta) \quad .$$

The angle θ is in the τ rest frame. This can be derived from the energy of the pion in the laboratory frame, E_π:

$$\cos\theta = \frac{2E_\pi/E_B - 1 - (m_\pi/m_\tau)^2}{1 - (m_\pi/m_\tau)^2} \quad .$$

The tau polarisation asymmetry, P_τ, is defined in terms of the cross sections for production of right-handed, σ_R, and left-handed, σ_L, tau leptons:

$$P_\tau = \frac{\sigma_R - \sigma_L}{\sigma_R + \sigma_L}$$

and in the Standard Model, assuming V-A couplings, it is given by:

$$P_\tau = \frac{-2\hat{g}_a^\tau \hat{g}_v^\tau}{\hat{g}_a^{\tau 2} + \hat{g}_v^{\tau 2}} \quad .$$

This depends only on the final-state couplings of the Z^0 to the τ. Hence, combining the measurement of P_τ with that of A_{FB}^{ll} and $\Gamma_{l^+l^-}$ gives a test of lepton universality and determines the sign of $\hat{g}_v^l/\hat{g}_a^l$. An example from the ALEPH Collaboration is shown in Fig. 16 and the combined LEP measurements are presented in Fig. 14 [8].

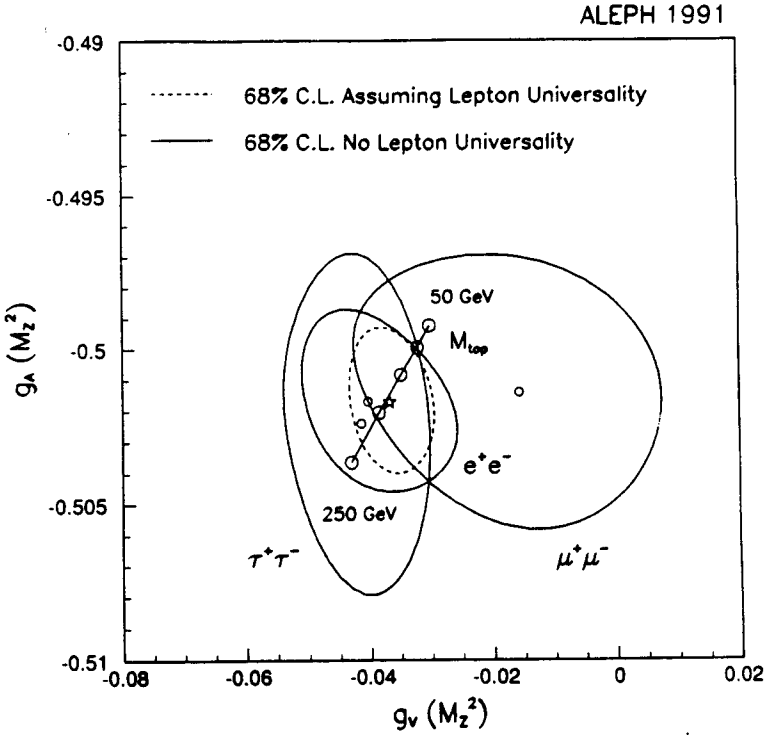

Figure 16: Determinations of $\hat{g}_a^l$ and $\hat{g}_v^l$ by the ALEPH Collaboration using the lepton pair forward-backward asymmetries and the τ polarisation asymmetry measured from 1991 data. The solid contours show e^+e^-, $\mu^+\mu^-$ and $\tau^+\tau^-$ couplings separately. The dashed contour shows the l^+l^- couplings, after assuming lepton universality. The line shows the prediction of the Standard Model for various choices of m_t.

1.7 Forward-Backward Asymmetry in $e^+e^- \to b\bar{b}$

This is in principle a very sensitive test of the Standard Model, because, compared to A_{FB} for lepton pairs, A_{FB} for $b\bar{b}$ pairs is large at $\sqrt{s} = M_Z$. Experimentally it is much more difficult to measure, since the $b\bar{b}$ events have to be separated from the general multihadronic background and the charge of the primary quark or antiquark has to be determined.

High momentum electrons and muons from semileptonic b decays are usually used to tag the $b\bar{b}$ events and measure the charge, with $\cos\theta$ coming from the thrust axis. A fit has to be performed to the $b\bar{b}$, $c\bar{c}$ and background components in the sample and uncertainties arise from the asymmetry of the $c\bar{c}$ events and the modelling of heavy quark decays, for example.

Having obtained a value for the observed $A_{FB}^{b\bar{b}}$, a correction has to be made for the effects of $B^0\overline{B^0}$-mixing in order to recover $A_{FB}^{b\bar{b}}$ at the parton level, which is what is needed to compare with the theoretical prediction.

$$A_{FB}^{b\bar{b}} = \frac{A_{FB}^{b\bar{b}}(\text{observed})}{1 - 2\chi_B}$$

where χ_B is the $B^0\overline{B^0}$ mixing parameter which has been measured at LEP using events with two semileptonic b decays.

The measurements of $A_{FB}^{b\bar{b}}$, as reported by the four LEP collaborations [9], are shown in Fig. 15. In this case the combined LEP result is not a simple average due to the complication of the $B^0\overline{B^0}$ mixing correction. Since each collaboration has used a different value of χ_B to correct their own result, then the observed $A_{FB}^{b\bar{b}}$ values, before correction for $B^0\overline{B^0}$ mixing, must be combined to get the LEP average. This is then corrected using a recently reported LEP average value of $\chi_B = 0.128 \pm 0.011$ [10] in order to give the final LEP result for $A_{FB}^{b\bar{b}}$.

1.8 Average Forward-Backward Asymmetry in $e^+e^- \to$ Hadrons

At the parton level, all $e^+e^- \to q\bar{q}$ channels should have a forward-backward charge asymmetry:

$$A_{FB}^{q\bar{q}}(\sqrt{s} = M_Z) \propto \frac{\hat{g}_a^e \hat{g}_v^e \hat{g}_a^q \hat{g}_v^q}{(\hat{g}_a^{e2} + \hat{g}_v^{e2})(\hat{g}_a^{q2} + \hat{g}_v^{q2})}$$

After fragmentation, hadronisation and decays the experiments observe jets, not partons, in the detectors. However, some information on the charge of the original parton can be recovered from the charges of the highest momentum tracks in a jet. This method relies on a comparison between data and Monte Carlo prediction and is sensitive to the details of the modelling of fragmentation, decays, etc., used inside the Monte Carlo generator. By using different Monte Carlo programs and different model parameter values an estimate of the systematic uncertainty can be made. It is the dominant error.

Within the Standard Model the couplings, and hence $A_{FB}^{q\bar{q}}$, of the up-type and down-type quarks are expected to be different. Hence, the value of $A_{FB}^{q\bar{q}}$ measured from all multihadronic events depends also on the relative production rates of the different quark flavours. The result has to be interpreted by comparison with the prediction of a program such as ZFITTER [6], and is normally expressed in terms of an "effective weak mixing angle," averaged over quark flavours:

$$\sin^2\overline{\theta}_W \approx \frac{1}{4}\left(1 - \frac{\hat{g}_v^q}{\hat{g}_a^q}\right)$$

The LEP results [11] are given in Table 1 together with a LEP average which has been evaluated on the assumption that all fragmentation and theoretical errors are completely correlated between the different experiments.

Experiment	$\sin^2\overline{\theta}_W$
ALEPH $\sin^2\theta_W(M_Z^2)$ DELPHI $\sin^2\theta_W^{eff}$ OPAL $\sin^2\theta_W^{eff}$	$0.2300 \pm 0.0034(\text{stat.}) \pm 0.0010(\text{syst.}) \pm 0.0038(\text{th.})$ $0.2345 \pm 0.0030(\text{exp.}) \pm 0.0027(\text{frag.})$ $0.2321 \pm 0.0017(\text{exp.}) \pm 0.0027(\text{frag.}) \pm 0.0009(\text{B mix.})$
LEP $\sin^2\theta_W(M_Z^2)$	$0.2324 \pm 0.0012(\text{exp.}) \pm 0.0031(\text{frag.})$

Table 1: Results for the effective weak mixing angle from the measurement of the $q\bar{q}$ forward-backward asymmetry. The definitions for $\sin^2\theta_W(M_Z^2)$ and $\sin^2\theta_W^{eff}$ differ slightly by the treatment of weak vertex corrections.

2. Tests of QCD at LEP

Quantum chromodynamics, the SU(3) sector of the Standard Model, has not been so precisely tested as the electroweak SU(2)×U(1) sector. In general, at LEP, QCD tests are limited by the theoretical systematic error, rather than by statistics.

Many features of QCD have been studied at LEP, including the flavour independence of α_S, evidence for gluon self-coupling, the gluon spin, quark-gluon jet differences and evidence for soft gluon coherence from particle spectra and the string effect.

In this review, only the determination of $\alpha_S(M_Z)$ and the consistency between different methods will be described. The data are taken from a recent report by S. Bethke and J.E. Pilcher [12] which should be consulted for the original sources.

2.1 Consistency of $\alpha_S(M_Z)$ Determinations

At LEP, $\alpha_S(M_Z)$ has been determined separately from the distributions of many different observables in multihadronic events, for example, various event shape parameters, jet masses, production rates of multijet events and correlations in energy or angle between particles in events.

For each of these observables a QCD calculation exists for the predicted distribution, up to $O(\alpha_S^2)$ in perturbation theory:

$$\frac{1}{\sigma_0}\cdot\frac{d\sigma}{dX} = \frac{\alpha_S(\mu)}{2\pi}A(X) + \left(\frac{\alpha_S(\mu)}{2\pi}\right)^2\left(A(X)2\pi\beta_0\ln(\mu^2/s) + B(X)\right)$$

where σ_0 is the lowest order cross section for $e^+e^- \rightarrow$ hadrons, $\beta_0 = 11 - \frac{2}{3}N_f$, N_f is the effective number of quark flavours ($N_f = 5$ at $\sqrt{s} = M_Z$) and $A(X)$ and $B(X)$ are functions of the observable under study, X. The strong coupling constant, $\alpha_S(\mu)$, is a function of the renormalisation factor, μ, which would be arbitrary if α_S could be calculated exactly. In a perturbative expansion up to $O(\alpha_S^2)$ the result still has a μ-dependence, due to the missing higher order terms. The so-called "natural scale" is $\mu^2 = s$, but values of μ^2 much less than s are thought to minimise the effects of the unknown higher order contributions. The choice of μ leads to a scale uncertainty in α_S.

The experimental statistical and systematic errors on α_S measurements at LEP are generally small ($\Delta\alpha_S = O(10^{-3})$) and cannot account for the spread of α_S values determined by different methods. For example, the α_S determinations of the OPAL Collaboration are shown in Fig. 17 [13].

The theoretical errors dominate. The hadronisation uncertainty, arising from the non-perturbative part of QCD, can be estimated by using different fragmentation models and parameters in the Monte Carlo programs used to compare with the data, giving $\Delta\alpha_S = O(10^{-3})$-$O(10^{-2})$ depending on the observable.

The scale uncertainty has to be estimated by varying $x_\mu = \mu/\sqrt{s}$ over some reasonable range. Different choices have been made by the different LEP collaborations in the presentation of their data, for example, $m_b/\sqrt{s} < x_\mu < 1$ (m_b is the bottom quark mass) or $\frac{1}{4} < x_\mu < 1$. The resulting errors are $\Delta\alpha_S = O(10^{-2})$, but the actual value can vary by a factor of two depending on the method used to estimate it. The choice of x_μ to use for the central value of α_S quoted is also somewhat arbitrary. When comparing results from different experiments they must first be adjusted so that they all conform to the same choice.

For the results given in this review the following method has been used. Firstly, an optimum value of $x_\mu = \mathrm{opt}(x_\mu)$ is found which gives the best fit between the theoretical prediction and the experimentally measured distribution, i.e., that value of x_μ which minimises the χ^2. To estimate the scale error on α_S, x_μ is allowed to vary over the range $\mathrm{opt}(x_\mu) < x_\mu < 1$ and the mean value of α_S for x_μ within this range is quoted as the central value.

Figure 18 shows the OPAL α_S values again after the theoretical uncertainties have been included. There is now good agreement. The errors on the different values are highly correlated, being dominated by the scale uncertainty. Figure 19 shows the α_S values determined by all LEP collaborations from different distributions, after having been adjusted to use the same definition of the scale uncertainty as described above. They are all consistent with one another, and a LEP average of $\alpha_S(M_Z) = 0.120 \pm 0.006$ has been derived. This consistency between $\alpha_S(M_Z)$ values determined from completely different distributions is a good verification of QCD.

In Fig. 20 are shown α_S measurements from many different types of experiments at energy scales ranging from the tau lepton mass up to the Z^0 mass. There is now good evidence for the running of α_S as predicted by QCD.

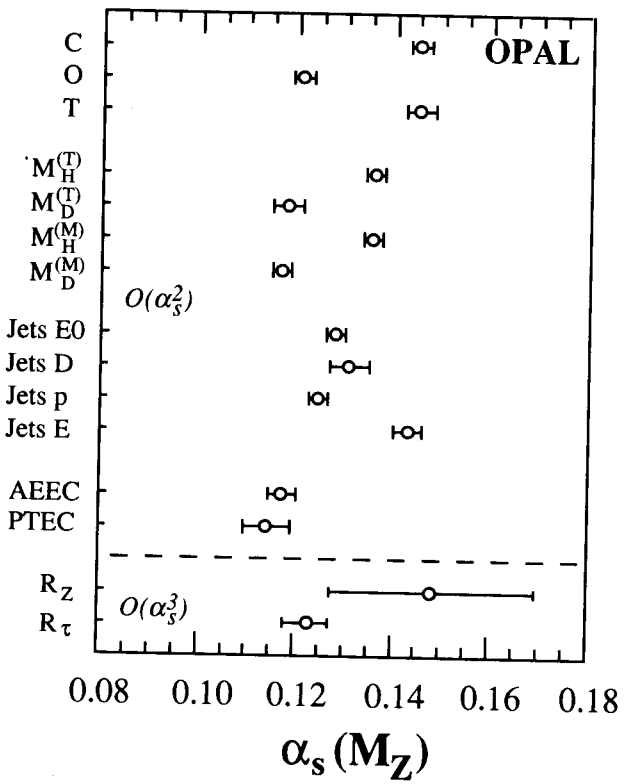

Figure 17: Compilation of measurements by the OPAL Collaboration of $\alpha_S(M_Z)$, for $\mu = M_Z$. See reference [13] for details of the different methods used. The errors shown are the statistical and experimental systematic uncertainties only. The discrepancies can be explained by including estimates of the theoretical systematic errors, see Fig. 18.

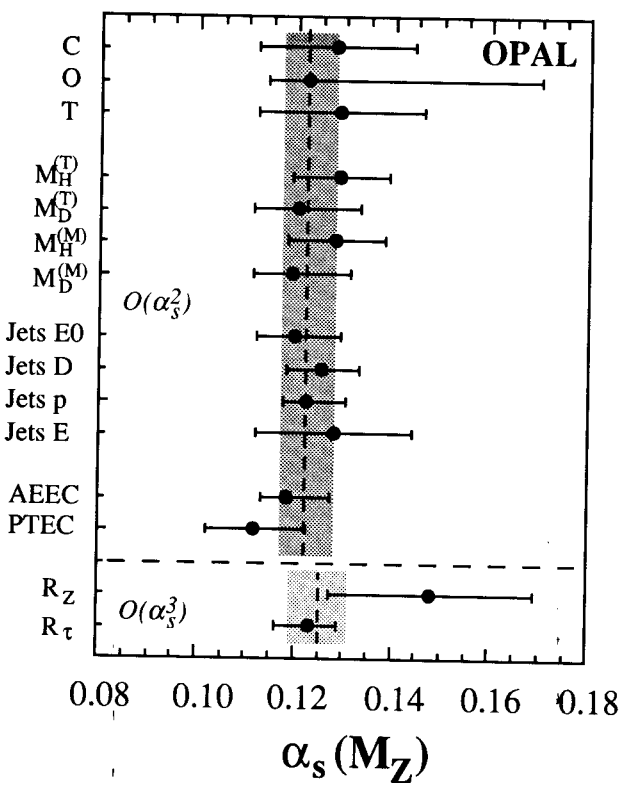

Figure 18: Compilation of final results for $\alpha_S(M_Z)$ from the OPAL Collaboration [13]. These are the same measurements as shown in Fig. 17, but after accounting for the theoretical errors. The different methods now give consistent results.

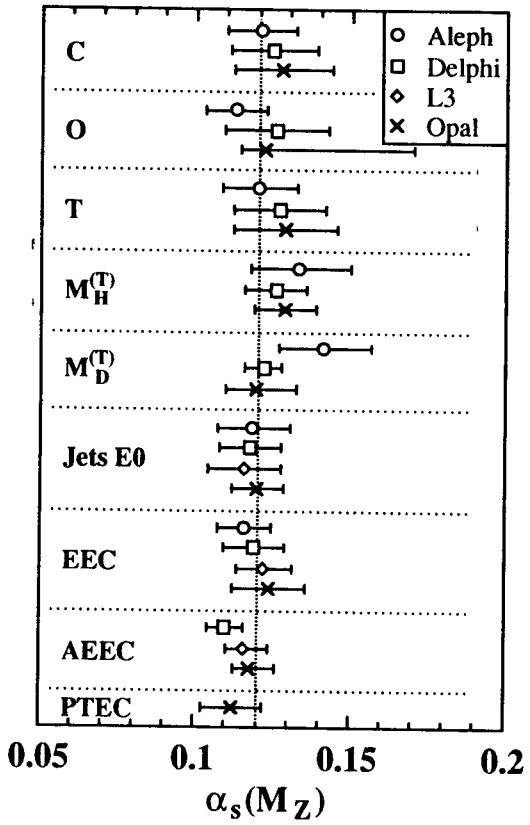

Figure 19: Compilation of LEP measurements of $\alpha_S(M_Z)$ at $O(\alpha_S^2)$ from event shapes, jet rates and energy correlations [12]. The errors contain the experimental and theoretical uncertainties.

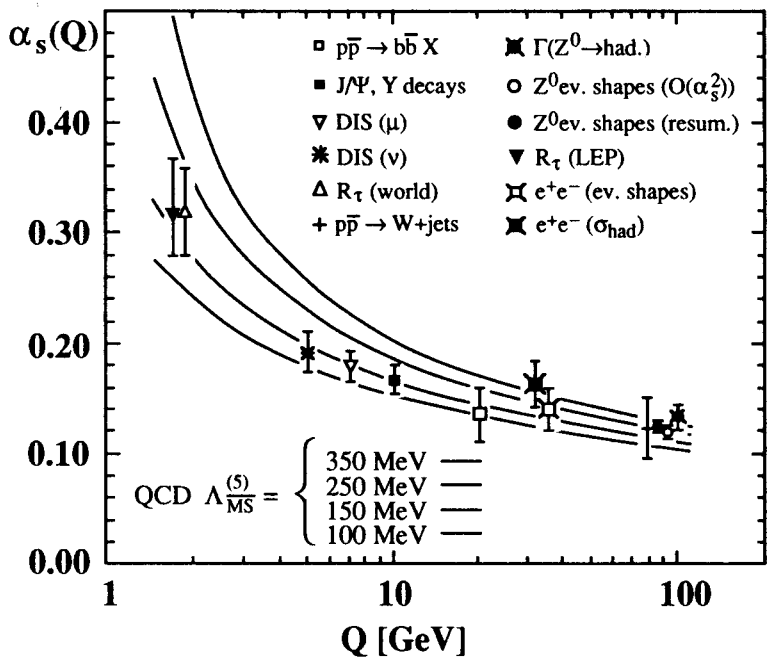

Figure 20: Compilation of measurements of α_S in the energy range from $\mu = m_\tau = 1.78$ GeV to $\mu = M_Z = 91.2$ GeV [12]. The open squares correspond to α_S determinations in next-next-to-leading order perturbation theory ($O(\alpha_S^3)$). The others are in next-to-leading order ($O(\alpha_S^2)$). The lines correspond to the QCD prediction of a running α_S for three values of $\Lambda_{\overline{MS}}$, expressed for five quark flavours above $\mu = 10$ GeV.

3. Overall Fit to LEP Data

In Section 1 it has been shown that, for all individual electroweak parameters measured, there is good agreement between the LEP experiments and consistency with the Standard Model. In this section, the combined dataset of electroweak measurements from LEP, along with some high-precision data from non-LEP experiments, is used to test the Standard Model and constrain its unknown parameters.

Fits have been performed using the ZFITTER program [6], with M_Z, m_t, M_H and α_S as free parameters, the input data are listed in Table 2. The values of m_t and α_S resulting from the fits are given in Table 3. In each case, the central value and first error results from a fit with M_H constrained to be 300 GeV, and the second error indicates the variation of the central value for M_H = 50 GeV and M_H = 1000 GeV.

In the first fit, only the LEP line shape and leptonic forward-backward asymmetry data are used. In the second fit, also the other LEP asymmetries are included: P_τ, $A_{FB}^{b\bar{b}}$ and $A_{FB}^{q\bar{q}}$. For the third fit, M_W measurements from $p\bar{p}$ colliders (M_W/M_Z from the UA2 Collaboration [14] and M_W from the CDF Collaboration [15]) and $\sin^2\theta_W$ from neutrino-nucleon scattering experiments (the CHARM and CDHS Collaborations [16]) are added to further constrain the Standard Model.

The $\alpha_S(M_Z)$ values from these fits are always somewhat larger than the value given in Section 2, which was derived from QCD studies. This is investigated in the fourth fit in which an additional constraint of $\alpha_S = 0.120 \pm 0.006$ [12] is included. This results in a slightly increased value for m_t, but still gives a good fit to the data. Hence, at the present level of precision, the larger value of α_S indicated by σ_{had}^{pole} is not a significant discrepancy.

Measurement	Result
a) LEP	
line shape and lepton asymmetries:	
M_Z	91.175 ± 0.021 GeV
Γ_Z	2.497 ± 0.007 GeV
σ_{had}^{pole}	41.13 ± 0.20 nb
$\hat{g}_a^{l\,2}$	0.2498 ± 0.0010
$\hat{g}_v^{l\,2}$	0.00124 ± 0.00024
+ LEP correlation matrix	
τ-polarisation:	
P_τ	-0.138 ± 0.021
$b\bar{b}$-asymmetry:	
$A_{FB}^{b\bar{b}}$	0.097 ± 0.011
$q\bar{q}$-asymmetry:	
$\sin^2\theta_W(M_Z^2)$ from $A_{FB}^{q\bar{q}}$	0.2324 ± 0.0033
b) $p\bar{p}$ and νN	
M_W/M_Z	$0.8813 \pm 0.0036 \pm 0.0019$
M_W	79.91 ± 0.39 GeV
$\sin^2\theta_W(\nu N)$	0.2300 ± 0.0064

Table 2: Precision measurements of Standard Model parameters included in the overall fit. Section a) combined LEP results from this review. Section b) results from hadron colliders and νN-scattering.

Input Data	m_t (GeV)	$\alpha_S(M_Z^2)$	χ^2/NDOF
a) LEP alone			
line shape + $A_{FB}^{l\bar{l}}$	$136^{+29\ +17}_{-38\ -19}$	$0.145 \pm 0.011 \pm 0.002$	$1.6/(5-3)$
$+P_\tau + A_{FB}^{b\bar{b}} + A_{FB}^{q\bar{q}}$	$149^{+23\ +17}_{-27\ -22}$	$0.142 \pm 0.011^{+0.002}_{-0.001}$	$2.2/(8-3)$
b) LEP all + UA2, CDF + CHARM, CDHS			
LEP $+M_W$ $+\sin^2\theta_W(\nu N)$	$\boxed{146^{+20\ +17}_{-22\ -21}}$	$\boxed{0.143 \pm 0.010^{+0.002}_{-0.001}}$	$3.0/(11-3)$
c) LEP all + UA2, CDF + CHARM, CDHS + $\alpha_S(M_Z^2) = 0.120 \pm 0.006$	$155^{+18\ +17}_{-20\ -22}$	$0.126 \pm 0.005 \pm 0.000$	$6.8/(12-3)$

Table 3: Results of top mass fits to data from LEP, UA2, CDF, CHARM and CDHS Collaborations. The central value and the first error refer to $M_H = 300$ GeV. The second error gives the variation of the central value for Higgs mass values spanning the interval $50 < M_H < 1000$ GeV. The value of α_S has not been constrained in these fits. Section a) summarises limits derived from LEP data alone. Section b) includes all LEP observables, M_W from UA2 and CDF and $\sin^2\theta_W$ from the νN-scattering experiments CHARM and CDHS. In Section c) the fit including all data has been repeated constraining the value of α_S to $\alpha_S = 0.120 \pm 0.006$.

4. Summary

The LEP data have allowed some precise tests of the Standard Model. There is good agreement between the four experiments and theory for all electroweak and QCD parameters studied. In an overall fit, the data are consistent with a radiatively corrected Standard Model and indicate an approximate range for the top quark mass of $m_t \approx 145 \pm 20 \pm 20(M_H)$ GeV.

Acknowledgements

I am grateful to my colleagues in the four LEP experimental collaborations and the LEP Accelerator Group who provided the data and helpful advice necessary to prepare this review. I thank D. Schaile and G. Quast for help with the Standard Model fits and S. Bethke for the review of α_S measurements. I would like to thank the organisers of the SLAC Summer Institute for their hospitality and assistance.

References

[1] LEP Polarization Collaboration, L. Arnaudon et al., Phys. Lett. B284 (1992) 431.

[2] Working Group on LEP Energy, L. Arnaudon et al., CERN-PPE/92-125 (1992).

[3] LEP Collaborations (ALEPH, DELPHI, L3 and OPAL), Phys. Lett. B276 (1992) 247.

[4] The results presented are preliminary. Details of the analysis techniques can be found in the following publications based on 1990 LEP data:
ALEPH Collaboration, D. Decamp et al., Z. Phys. C53 (1992) 1;
DELPHI Collaboration, P. Abreu et al., Nucl. Phys. B367 (1991) 511;
L3 Collaboration, B. Adeva et al., Z. Phys. C51 (1991) 179;
OPAL Collaboration, G. Alexander et al., Z. Phys. C52 (1991) 175.

[5] M. Consoli and W. Hollik, Z. Physics at LEP1, CERN 89-08, ed. G. Altarelli et al., Vol. 1 (1989) 7.

[6] ZFITTER program: D. Bardin et al., Z. Phys. C44 (1989) 493, Nucl. Phys. B351 (1991) 1, Phys. Lett. B255 (1991) 290, CERN-TH.6443/92 (1992).
MIZA program: M. Martinez et al., Z. Phys. C49 (1991) 645.
ALIBABA program: W. Beenakker et al., Nucl. Phys. B349 (1991) 323.

[7] E. Gross, CERN-PPE/92-91 (1992).

[8] The results presented are preliminary. Details of the analysis techniques can be found in the following publications:
ALEPH Collaboration, D. Decamp et al., Phys. Lett. B265 (1991) 430;
DELPHI Collaboration, P. Abreu et al., CERN-PPE/92-60 (1992);
L3 Collaboration, O. Adriani et al., CERN-PPE/92-132 (1992);
OPAL Collaboration, G. Alexander et al., Phys. Lett. B266 (1991) 201.

[9] The results presented are preliminary. Details of the analysis techniques can be found in the following publications:
ALEPH Collaboration, D. Decamp et al., Phys. Lett. B263 (1991) 325;
DELPHI Collaboration, P. Abreu et al., Phys. Lett. B276 (1992) 536;
L3 Collaboration, O. Adriani et al., CERN-PPE/92-121 (1992);
OPAL Collaboration, M.Z. Akrawy et al., Phys. Lett. B263 (1991) 311.

[10] M. Hebert, UCSD/L3, talk at "Beyond the Standard Model '92" conference, Carleton University, Ottawa, Canada, 23 June 1992.

[11] ALEPH Collaboration, D. Decamp et al., Phys. Lett. B259 (1991) 377;
DELPHI Collaboration, P. Abreu et al., Phys. Lett. B277 (1992) 371;
OPAL Collaboration, P.D. Acton et al., CERN-PPE/92-119 (1992).

[12] S. Bethke and J.E. Pilcher, HD-PY 92/06 (1992) or EFI 92-14, Annual Review of Nuclear and Particle Science, Vol. 42 (1992).

[13] OPAL Collaboration, P.D. Acton et al., Z. Phys. C55 (1992) 1.

[14] UA2 Collaboration, J. Alitti et al., Phys. Lett. B276 (1992) 354.

[15] CDF Collaboration, F. Abe et al., Phys. Rev. Lett. 65 (1990) 2243, Phys. Rev. D43 (1991) 2070.

[16] A. Blondel et al., Z. Phys. C45 (1990) 361;
CHARM Collaboration, J.V. Allaby et al., Z. Phys. C36 (1987) 611.
The average value for $\sin^2\theta_W$ has been scaled to $m_t = M_H = 100$ GeV as in:
CHARM-II Collaboration, D. Geiregat et al., Phys. Lett. B259 (1991) 499.